International Journal of Heat and Fluid Flow 119 (2026) 110331

Contents lists available at ScienceDirect

International Journal of Heat and Fluid Flow

journal homepage: www.elsevier.com/locate/ijhff

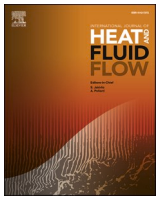

Design of micro-channel based actively cooled thermal shields for ultra-high temperature applications

Pedro Miranda [a,*], Rafael Agujetas [a], José M. Montanero [a], Florencia M. Nogales [a], Abdulnaser Sayma [b]

[a] Departamento de Ingeniería Mecánica, Energética y de los Materiales, Universidad de Extremadura, Badajoz, Spain
[b] College of Engineering, Design and Physical Sciences, Brunel University of London, Kingston Lane, Uxbridge, Middlesex UB8 3PH, United Kingdom

ARTICLE INFO

Keywords:
Ultra-high temperature thermal shields
Active cooling
Microchannels
Ultra-high temperature ceramics

ABSTRACT

In this study, novel designs of high-temperature thermal shields that can be actively cooled by circulating water through a bioinspired internal microchannel network are numerically evaluated. The level of cooling that can be achieved and the thermal stresses developed in the shield material are analysed using computational fluid dynamics and finite element modelling. From the comparative analysis of those results, design guidelines for the development of such actively cooled thermal shields (ACTS) are proposed: (i) channel design plays only a minor role on the coolant mass needed to produce a desired level of cooling but (ii) small channels around the regions of maximum temperature gradient and stress concentrators like sharp corners should be avoided to prevent cracking of the shield material; and (iii) high temperature tolerance and high thermal conductivity are key parameters for the shield material. Thus, ultra-high temperature ceramics (UHTC) such as ZrB_2 appear to be optimal candidates for the additive fabrication of such ACTS elements, provided they can survive the thermal cycling without cracking. Water was confirmed as an excellent coolant for such an application, enabling the development of reusable solutions for aerospace re-entry shields, involving coolant masses that could become competitive against current single-use ablative shields. Similar systems could provide suitable thermal protection or heat exchange solutions in many other demanding industrial applications.

1. Introduction

Aerospace applications involving descending into planetary atmospheres, including re-entry into Earth's atmosphere which is critical for reusable space vehicles, and hypersonic flight require the use of Ultra-High Temperature Materials (UHTMs) capable of protecting both vehicles and crew members from extreme temperatures (exceeding 1600 °C) and severe environments (highly erosive, corrosive, plasmas, etc.). Similar stringent requirements are found in scramjet and rocket propulsion components, as well as multiple pyrochemical and energy reactors, including nuclear fusion prototypes under development. Aerospace applications are especially demanding since the weight and energy consumption of the thermal protection system (TPS) on the vehicle must be minimized to reduce fuel consumption and maximize payload. A variety of UHTMs are being considered for these demanding applications. Only a handful of refractory transition metals with melting points above 2000 °C (Nb, Mo, Ta, W and Re) and their alloys are considered to be suitable for these purposes. However, even the most refractory metals and superalloys, typically require the use of passivating ceramic coatings to prevent oxidation and subsequent performance degradation. Thermal spray coatings, typically referred to as thermal barrier coating (TBCs), are extensively used for retarding the material degradation due to higher heat flux (Schütze, 2000). Making the thermal expansion of the two materials mutually compatible is a challenge and often an intermediate metallic bond coat is used to reduce residual stresses generated during deposition. However, even the most successful TBCs can fail under extreme heat and corrosive environments. The prominent mode of degradation in a TBC is the oxidation of the bond coat leading to the formation of thermally grown oxide (TGO) and subsequent generation of stresses due to thermal expansion mismatch (Thakare et al., 2020).

The aforementioned limitations and the drive towards ever increasing service temperatures have led to the development of ultra-high temperature ceramic (UHTC) alternatives: ceramic materials with

* Corresponding author.
E-mail address: pmiranda@unex.es (P. Miranda).

https://doi.org/10.1016/j.ijheatfluidflow.2026.110331
Received 13 October 2025; Received in revised form 13 January 2026; Accepted 21 February 2026
Available online 26 February 2026

melting points above 3000 °C, which can be suitable for structural applications above 2000 °C. Some borides, nitrides and carbides of the group IV B and V B transition metals (ZrB_2, TiB_2, HfB_2, ZrC, HfC, TaN, etc.) belong to this category (Golla et al., 2020; Justin and Jankowiak, 2011; Fahrenholtz and Hilmas, 2017). These materials exhibit an excellent combination of high melting point, hardness, elastic modulus, good wear resistance, electrical and thermal conductivity, good creep resistance and chemical stability (Rao Bakshi, 2016). Their main drawback lies in their poor sinterability and intrinsic brittleness. In this regard, advanced sintering techniques (e.g. SPS) and the use of sintering additives have been successfully employed to obtain dense UHTCs (Zamora et al., 2012; Zamora et al., 2012) and particle/fibre reinforcements have been used to produce tougher and stronger UHTC composites (Sciti et al., 2014). It is even possible to find multifunctional additives (SiC, ZrC, $MoSi_2$, $TaSi_2$, Si_3N_4 as examples) acting simultaneously as sintering aids, mechanical reinforcements and even improving the already significant UHTCs oxidation resistance (Dehdashti et al., 2014; Hu et al., 2010; Huo et al., 2018).

However, despite all these efforts, service lifetime of every UHTM is still limited by their thermochemical degradation under the extremely hot, corrosive and ablative environments they must endure in their intended applications. The only solution for extending their durability is to resort to active cooling of the part. This is done routinely in turbine blades in gas turbines, where around 20% of the cold compressor air is bled off for cooling the interior of the blade and vented through small holes onto the blade aerofoil surface, especially near the leading edge. Ideally, the cooling air emerges at low velocity, forming a protective cooling film around the blade in a process commonly referred to as *film cooling* or *transpiration cooling* (Hermann et al., 2019; Shine and Nidhi, 2018). When the coolant used for this type of active cooling is in liquid form and evaporates as it is ejected to the exterior, the process is known as *evaporative cooling*. Such a method possesses additional cooling efficiency as it can benefit from the enthalpy of vaporization of the cooling media to further dissipate incoming heat flux. However, most of the active cooling is currently performed at the system (macroscopic) level, where the surface area available for heat exchange between the coolant and the UHTM is limited. This study proposes to use additive manufacturing (AM) to produce shield elements possessing an intricate internal microchannel network capable of providing a high surface area for heat exchange between the shield material and an appropriate coolant. This constitutes a significant innovation over existing use of AM for ultrahigh temperature thermal shields, since most existing research effort is limited to the 3D printing of single-use ablative TPS materials (Kennedy et al., 2024; Badea et al., 2025; Olson et al., 2023; Blette et al., 2024) or creating passive insulating structures (Mei et al., 2023; Raisch, 2020) or internal hollow cores (Ferrari et al., 2016) rather than using its freeforming capabilities to produce reusable shields through optimally-designed active cooling. Indeed, the cooling fluid circulated through the microchannels of the proposed actively cooled thermal shield (ACTS) at an appropriate flow rate could significantly reduce the material temperature, dramatically delaying its corrosion and reducing performance degradation over multiple cycles. This design is bioinspired, mimicking the bed of capillaries found in plant leaves or at the surface of the skin in most animals, which plays a critical role in the thermoregulation of their bodies. Similar strategies have already been proposed and successfully demonstrated for the refrigeration of windows, solar panels and electronic devices (Hatton et al., 2013; Tao et al., 2015; Van Erp et al., 2020) but, up to date, not for high temperature applications.

The proposed ACTS can be fabricated using ultra-high temperature ceramics (Nogales, xxxx; Sández-Gómez et al., 2025) or refractory metals through different additive manufacturing technologies: Slurry-based techniques such as Direct Ink Writing (DIW) and Digital Light Processing (DLP) could be used for the deposition of UHTCs; while powder-based Directed Energy Deposition (DED) and Powder Bed Fusion (PBF), could be used to produce metallic-based ACTS. Moreover, AM procedures enabling the fabrication of ACTS using a combination of both types of materials and/or graded ceramic/metal structures could be developed. Using hybrid compositions will enable combining the best properties of each material: the high melting point and chemical stability of the UHTCs with the higher toughness and thermal conductivity of the metallic materials. The fabrication of ceramic/metal parts has already been demonstrated by either using a single AM technique (Scheithauer et al., 2015) or by hybridizing two different ones (Raynaud et al., 2021). Work is underway within AM-ACTS M-ERA.NET project (Miranda, 2021) for the fabrication of both the single-material and hybrid ACTS with preliminary promising results. However, before such high-temperature TPS can be successfully developed, it is necessary to understand their behaviour under relevant conditions and to optimize the design of their internal microchannel network. This is the main purpose of the current study, where an initial simple prototype ACTS system is analysed with the aid of numerical simulations, both by using computational fluid dynamics (CFD) to analyse the solid/fluid thermal exchange problem and finite element analysis (FEA) to study the developed thermal stresses. The effect of different coolants, mass flow rates, channel network designs and materials on the developed temperature profiles in the prototype ACTS system is comparatively studied and relevant design guidelines for this type of TPS are extracted. Optimized ACTS may find applications in various fields like aerospace, solar thermal energy harvesting and storage, as well as in nuclear energy and chemical industries.

2. Computational model and numerical simulations

2.1. General model description

Computational fluid dynamics (CFD) and finite element modelling (FEM) simulations of ACTS prototypes were performed using the commercial software ANSYS®, which enabled finding numerical solutions for both the solid/fluid heat exchange problem and the thermo-mechanical stress field developed in the TPS during the process. As shown in Fig. 1, a simple three-dimensional model was used to simulate the heating of a thermal shield disk-shaped element, subject to an intense frontal heat flux of 1 MW/m^2, emulating the demanding conditions of an atmospheric re-entry. Adiabatic boundary conditions were applied to the remaining surfaces of the ACTS, simulating a worst-case scenario in which the shield element cannot dissipate any heat to the surrounding environment, which could be representative of an individual heat shield element surrounded by similar elements at the same temperature and perfectly insulated at the back. In this way, the ACTS element can be exclusively cooled through an internal network of

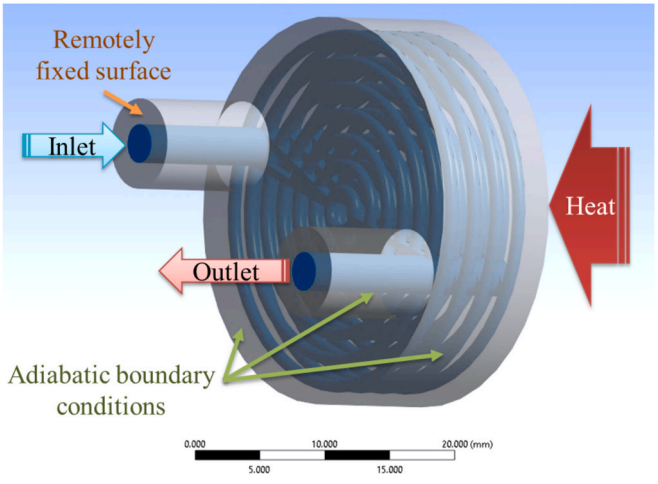

Fig. 1. Three-dimensional model used to simulate the actively cooled thermal shield (ACTS) prototype tiles subject to a frontal heat flux (1 MW/m^2) in the order of those developed during Earth atmospheric re-entry.

Table 1
Thermophysical properties of solid and fluid materials used in the numerical simulations.

Material	Property	Polynomial coefficients $a_0 + a_1 T + a_2 T^2 + a_3 T^3 + a_4 T^4$					Units
		a_0	a_1	a_2	a_3	a_4*	
Steam (Ernst, 1986)	Thermal cond., κ	0.02243541	−7.987145 ·10^{-5}	2.996699 ·10^{-7}	−1.997298 ·10^{-10}	5.454112 ·10^{-14}	W/m K
	Heat capacity, C_p	1563.007	1.603755	−2.932784 ·10^{-3}	3.216101 ·10^{-6}	−1.156827 ·10^{-9}	J/K
	Viscosity, η	1.908226 ·10^{-5}	−8.472089 ·10^{-8}	2.556141 ·10^{-10}	−2.220173 ·10^{-13}	6.957573 ·10^{-17}	kg/m s
Water (Ernst, 1986)	Density, ρ	998.2					kg/m^3
	Thermal cond., κ	0.6					W/m K
	Heat capacity, C_p	4182					J /K
	Viscosity, η	0.001003					kg/m s
ZrB_2	Density, ρ	6290					kg/m^3
(Grohsmeyer et al., 2019; Zimmermann et al., 2008; Lugovy et al., 2016; Nakamori et al., 2015);	Thermal cond., κ	54.818	0.0073				W/m K
	Heat capacity, C_p	593.389631	5.020125 ·10^{-2}	1.270651 ·10^{-5}	−1.344000 ·10^{-9}	1.626995 ·10^{4} *	J/K
	Thermal exp. coeff., α	−16	1.72 ·10^{-3}	−2.31 ·10^{-7}			μm/m/K
	Elastic modulus, E	473.93252	−0.03662				GPa
	Poisson's ratio, υ	0.13769	1.12665 ·10^{-5}				
Inconel	Density, ρ	8190					kg/m^3
(K.C. Mills, Ni-IN718, in: Recommended values of thermophysical properties for selected commercial alloys, 2002; Davis, 2000)	Thermal cond., κ	1.79762	0.02587	−4.89241 ·10^{-6}			W/m K
	Thermal exp. coeff., α	9.37926	0.01743	−2.40717 ·10^{-5}	1.29543 ·10^{-8}		μm/m/K
	Heat capacity, C_p	372.76	2.27831	−2.52568 ·10^{-5}			J/K
ZrO_2 (Radovic et al., 2008; Limarga and Clarke, 2011)	Density, ρ	5680					kg/m^3
	Thermal cond., κ	0.87591	0.0052	−8.2163 ·10^{-6}	5.74264 ·10^{-9}	−1.486828 ·10^{-12}	W/m K
	Heat capacity, C_p	−0.00589	0.026957	−3.79829 ·10^{-6}	2.77509 ·10^{-9}	−7.60272 ·10^{-13}	J/K

* a_4 coefficient for ZrB_2 Cp corresponds to an inverse term ($a_4 T^{-1}$) instead of a 4th order polynomial term ($a_4 T^4$).

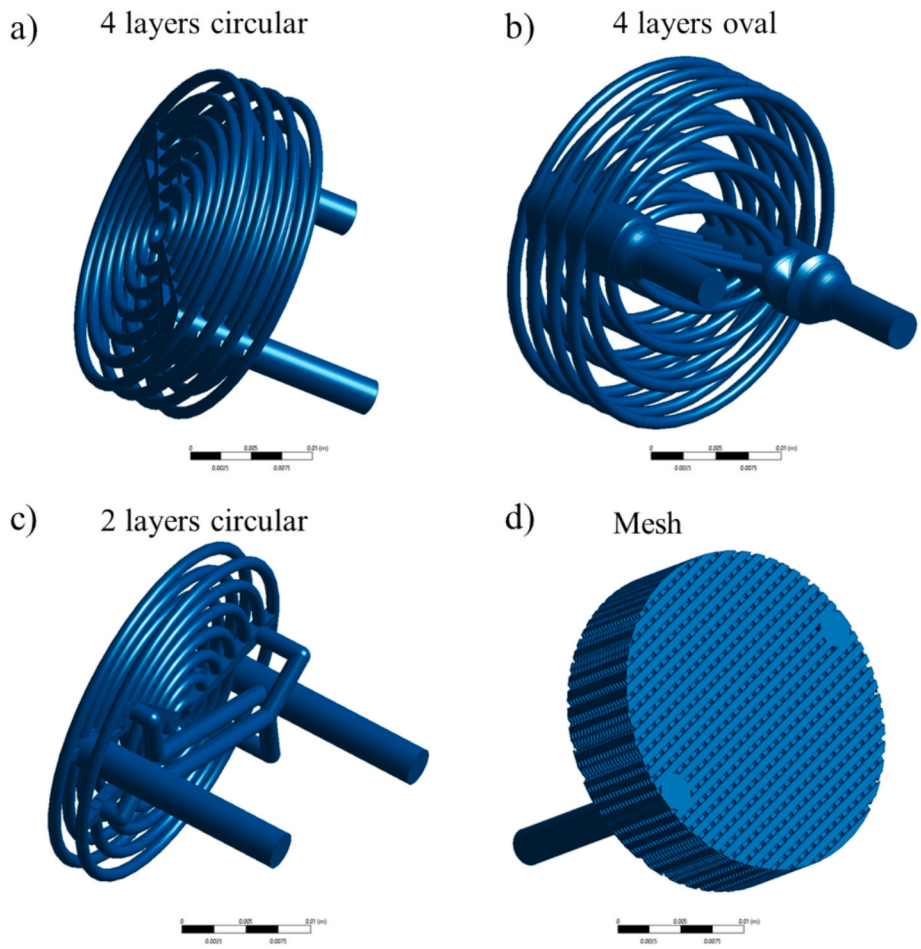

Fig. 2. Internal microchannel designs analysed in this work, with selected denomination as indicated. All channels are 1 mm minimum size with circular (a-c) or square (d) transversal sections. Coolant circulation occurs in opposite directions for each channel layer in c) but is unidirectional, from inlet to outlet, in the rest.

microchannels embedded into the solid material and connected to inlet/outlet pipes located at its back. The selected geometry and boundary conditions were chosen as a stringent benchmark for the different materials and channel designs to be analysed. By restricting other potential heat sinks, temperature levels such as those reached in aerospace applications at similar incoming heat fluxes could be reproduced, and the relative effectiveness of each material/channel design could be evaluated. Accordingly, the absolute values of the results obtained in this study should not be considered representative of any specific real situation, without jeopardizing the conclusions that can be derived from the comparison of the obtained results across systems.

An inlet manifold distributes the coolant into multiple levels of parallel channels and the different fluid streams are gradually collected at the opposite side manifold and ejected through the outlet. External dimensions of the ACTS were 30 mm external diameter and 10 mm thickness for the disk, while the pipes were 10 mm in length, with internal and external diameters of 3 and 7 mm, respectively.

For the CFD simulations, a double-precision, pressure-based algorithm solving the Reynolds-averaged Navier Stokes equations and the energy equation. An absolute velocity formulation was used for the calculations, neglecting gravity effects. Water in liquid and steam phases were chosen as cooling fluids due to their excellent thermal properties and the fact that water might be readily available in spacecrafts, as it can also be used for life-support and as radiation shielding material. Initially, a single-phase model was used for the water vapour and the inlet temperature was set to 393.4 K to ensure physically consistent results at the selected pressure range (0.1–2 bar). Assuming vapour already at the inlet greatly simplifies the numerical modelling, which enables testing various materials and designs faster and avoiding convergence issues. The standard k–epsilon model turbulence was selected for the fluid domain. The Reynolds number was low, and hence the flow was deemed laminar in most cases. However, using the Reynolds Averaged Navier-Stokes equations with a turbulence model for the laminar cases showed similar results compared to those when the laminar flow model was used and, hence, the former was used for all cases for consistency. Steam density was calculated considering a real gas Soave-Redlich-Kwong equation of state and key thermodynamic properties were temperature dependent through a polynomial modelling of vapour tables (Ernst, 1986), as detailed in Table 1.

Constant pressure conditions were imposed at the inlet, defined as an input parameter for the simulation. The standard outflow boundary condition was prescribed at the outlet. The effect of material and coolant, as well as that of microchannel design and inlet pressure, on the stationary-state temperatures developed in the ACTS system was analysed. As shown in Fig. 2, four internal microchannel designs for coolant circulation were tested: the two first designs consisted of 4 layers of circular (Fig. 2a) or oval (Fig. 2b) 1 mm diameter circular channels, the third reduced the number of layers to 2 but incorporate features allowing the liquid to circulate in opposite directions in each of the layers (Fig. 2c) and the fourth had a orthogonal mesh of 1 mm interconnected square channels (Fig. 2d) instead. The interconnected 3D network of square channels in Fig. 2d is formed by alternating orthogonal layers of square-section 1 mm walls occupying the whole disk volume; and this mesh was enclosed by an external lateral wall of 2 mm thickness. Various materials (ZrB_2, Inconel 718 and ZrO_2) were analysed as potential constituents for the ACTS part. Their thermophysical

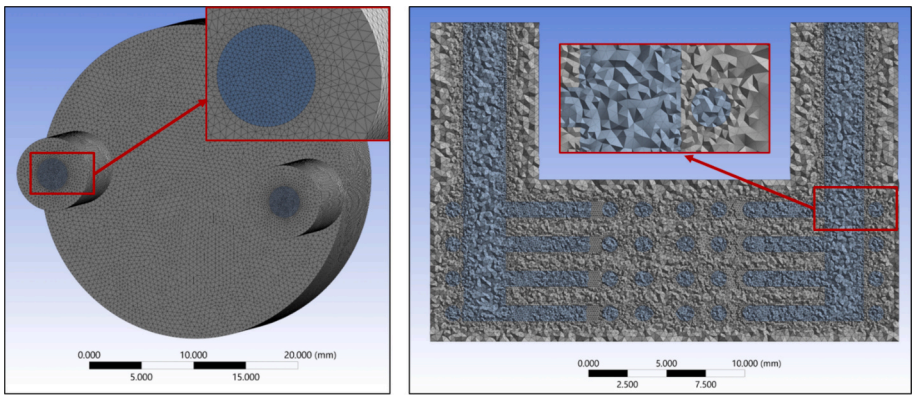

Fig. 3. Example of a 3D mesh used in CFD simulations for a model with 4 circular channel levels (7 channels per level).

properties, which were modelled based on existing literature reports (Grohsmeyer et al., 2019; Zimmermann et al., 2008; Lugovy et al., 2016; Nakamori et al., 2015; Mills, 2002; Davis, 2000; Radovic et al., 2008; Limarga and Clarke, 2011), are also defined in Table 1. Standard wall functions were used to simulate the solid–fluid interface.

For selected conditions, the calculated steady-state temperature distributions were used as input parameters for the FEM simulation to determine the thermal stresses developed in the ACTS part as a consequence of the heat exchange. For such numerical simulations, the body temperatures calculated in the CFD analysis were used as imported load, and a remote zero displacement boundary condition was imposed on the external facet of the inlet pipe (as schematically indicated in Fig. 1) to prevent any rigid body motion of the part. The inlet facet remained deformable to avoid introducing any additional stresses in the material due to the applied boundary condition.

Given the high temperatures expected in the shield during an atmospheric re-entry, vaporization is expected to occur and water vapour will be the fluid circulating through most of the channel network in the application. However, liquid water is a much better coolant than steam, being capable of absorbing larger amounts of heat thanks to its extremely high heat capacity and latent heat of vaporization. Thus, ignoring the heat absorption produced during such evaporation only provides a very conservative estimate of the level of cooling that can be achieved by using liquid water at a lower initial temperature at the inlet as coolant. Although multiphase simulations are prone to convergence issues and are often much less reliable in terms of accuracy, the two-layer microchannel network design (Fig. 2c) was used to perform an evaluation of the cooling efficiency of liquid water for this application. The volume of fluid (VOF) multiphase model (Hirt and Nichols, 1981) was used for this purpose, imposing a constant mass flow rate of liquid water at a temperature of 273.15 K at the inlet. Liquid water properties were assumed to be constant to simplify modelling and avoid convergence issues and the Lee evaporation/condensation model (Lee, 2013) was used to simulate the phase transition. ANSYS®'s default value of 0.1 s^{-1} was used for the Lee model's mass transfer intensity factor (Chen et al., 2020), and a constant saturation temperature of 373.15 K was considered in the simulations. The continuum surface stress model was used for modelling surface tension force at the interphase, with a surface tension coefficient of 0.059 N/m for water/vapour (Chen et al., 2020). A standard turbulence (k–epsilon) model was selected for the multiphase fluid with a default turbulence stabilization factor of 10 to facilitate convergence.

2.2. Mesh

An example of the CFD and finite element unstructured meshes used in this study is shown in Fig. 3. Quadratic tetrahedral elements were used for the CFD and FEM simulations. A global mesh size of 0.35 mm, with finer elements of around 0.13 mm along the solid/fluid boundary, was selected for the model, which resulted in meshes with over 7.5 million elements. This mesh configuration was selected after a suitable mesh independence study, which showed that any additional mesh

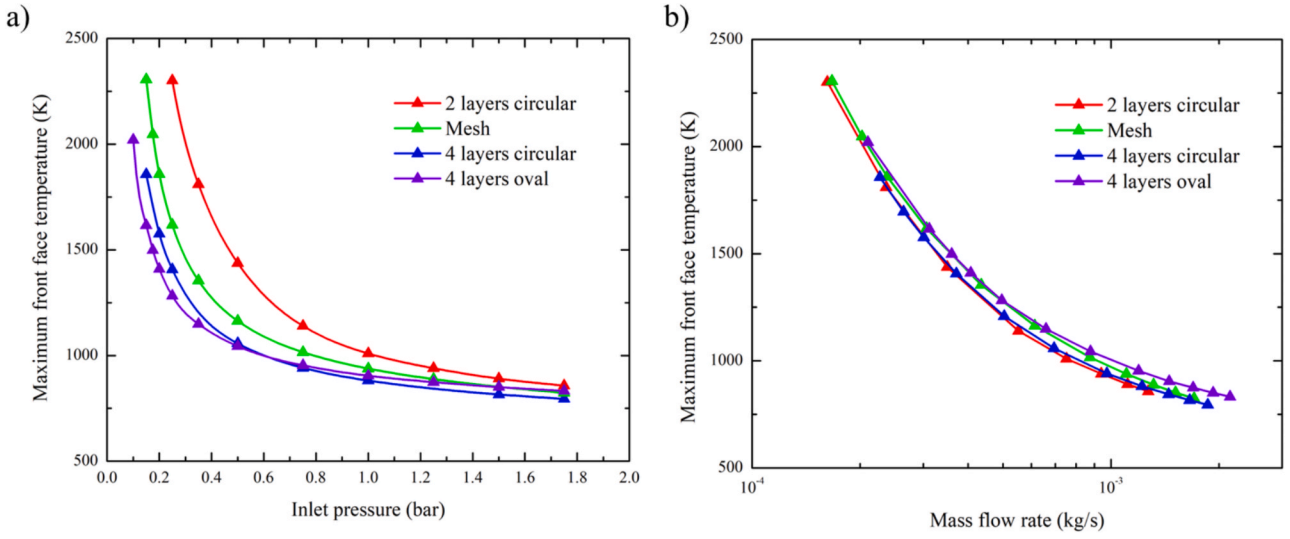

Fig. 4. Maximum temperature at the front face of a ZrB_2 ACTS as a function of the a) inlet pressure and b) mass flow rate of the dry steam used as a coolant for the indicated microchannel designs (cf. Fig. 2).

refinement produced variations on the model steady-state temperature distribution of less than 2%, in the worst case. Relatively low average values of Y^+ around 5 were evaluated for these meshes, which, given the relative coarseness of the mesh, are consistent with a laminar or quasi-laminar behaviour.

An appropriate experimental validation of our numerical predictions would involve reproducing experimentally the complex boundary conditions at the shield's front surface, where an extremely high heat flux is imposed, a difficult task that is beyond the scope of this work. However, the CFD simulations obviously verify the global mass and energy conservation equations. Therefore, measuring only thermodynamic and fluid dynamic parameters at the inlet and outlet section does not constitute a proper validation, which would require comparing numerical predictions for the temperature and gas velocity inside the shield with experimental values. Despite these limitations, our simulations constitute a useful guide for designing actively cooled thermal shields. Although there may be certain discrepancies between the absolute values predicted by the model and the real ones, the comparison between the different geometries and parameter configurations considered in our analysis is expected to be valid.

2.3. Evaluated parameters and scope of the study

The main output parameters that were evaluated in the CFD simulations were the temperature distributions in the TPS model, especially the maximum and average temperatures at the front and back faces and the mass flow rate of coolant. In the multiphase simulations, the average volume fractions of water/steam and the average pressure at the inlet were also evaluated for each condition. Maximum tensile stresses in the solid were considered the main output parameter in the finite element simulations as it is the critical parameter for determining failure in the samples when ultra-high temperature ceramics like ZrB_2 are selected for TPS fabrication.

At this point, it is worth highlighting that the present work is intended as a feasibility study of the proposed actively cooled microchanneled thermal protection systems and as a comparative analysis of different designs and potential material candidates for its fabrication. Therefore, the boundary conditions and individual material properties selected, as described in the preceding subsections, and their potential accuracy at representing actual system performance, are of secondary relevance. Indeed, while those input parameters can obviously affect the absolute values obtained for the different performance parameters, they will not qualitatively affect the trends observed upon variation of the design parameters and material properties and, thereby, do not jeopardize the validity of the subsequently derived conclusions. Thus, the most relevant outcomes of this study are the proposed design guidelines based on this comparative study.

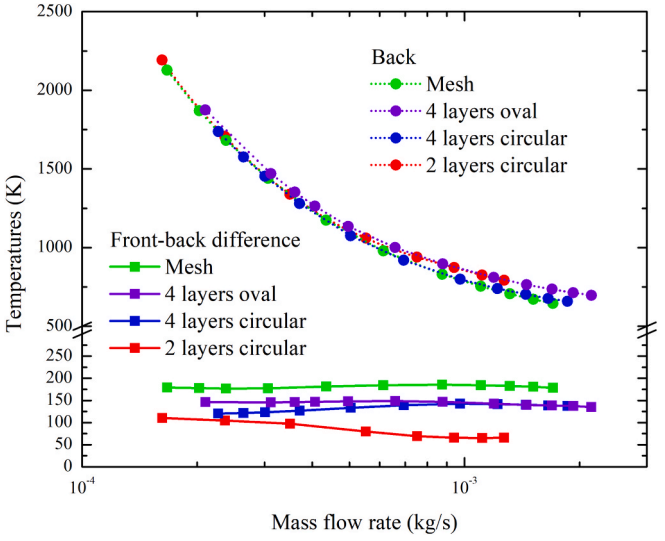

Fig. 5. Maximum temperature at the back face of a ZrB_2 ACTS and difference in the maximum temperature between the front and back faces as a function of the mass flow rate of the dry steam used as a coolant for the indicated microchannel designs (cf. Fig. 2).

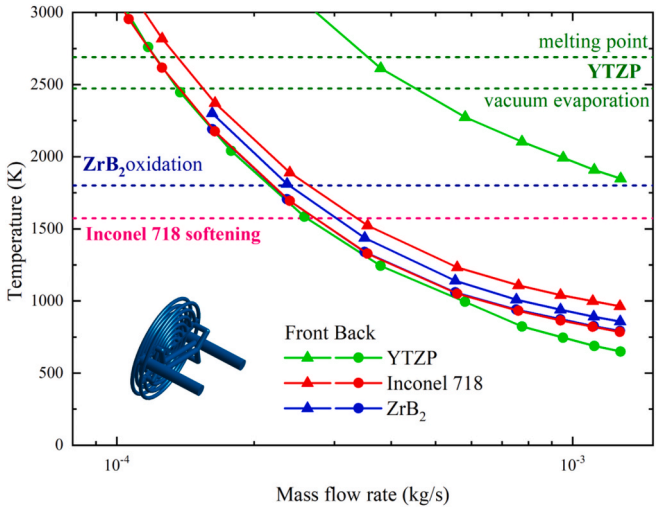

Fig. 6. Maximum temperature at the front face of the 2 layers circular ACTS design as a function of the mass flow rate of dry steam for different materials, as indicated. Different maximum temperature thresholds for usage of ZrB2 are indicated as horizontal lines.

3. Results and discussion

Regarding the microchannel network designs, Fig. 4 summarizes the results of CFD simulations performed with dry steam as coolant in terms of the maximum temperatures at the front face, the one receiving the incoming heat flux of 1 MW/m^2, of a ZrB_2 ACTS part. According to the results in Fig. 4a, designs with 4 layers of uniform channels perform better at reducing the temperature of the TPS at a given inlet pressure. However, the mass of coolant circulating rather than its pressure is the most critical parameter, especially in aerospace applications. When the same results are plotted as a function of the mass flow rate, as shown in Fig. 4b, it becomes clear that differences among the different designs are much less significant. In fact, according to this figure, the design with only 2 layers of microchannels seem to give the best performance despite having the lowest surface area for heat exchange between the solid and the cooling fluid. This is attributed to a more uniform temperature distribution at the front surface of the ACTS, which was achieved through the circulation of the coolant in opposite directions in each of the layers of this design. Thus, an ACTS system with the 2 layers circular design will require higher pressures to produce a certain level of cooling but will use less mass of coolant per unit time than the rest of the designs analysed.

As shown in Fig. 5, the incorporation of additional layers of channels allows a greater reduction of the maximum temperature at the back surface of the TPS, with the mesh and 4–layer circular designs giving the best results. However, the difference between designs only becomes significant as the mass flow rate increases and, at the lower rates, the system performance is very similar regardless of the number of layers in the design, which is also true for the temperatures at the front face (Fig. 4b). Differences between the temperatures at the front and back layers are nonetheless relatively small, under 200 °C for all cases, due to the high thermal conductivity of ZrB2. Temperature differences seem to grow slightly with the flow rate for all designs and then slowly decline, with the sole exception of the 2-layer design in which the difference seems to be reduced at faster flows.

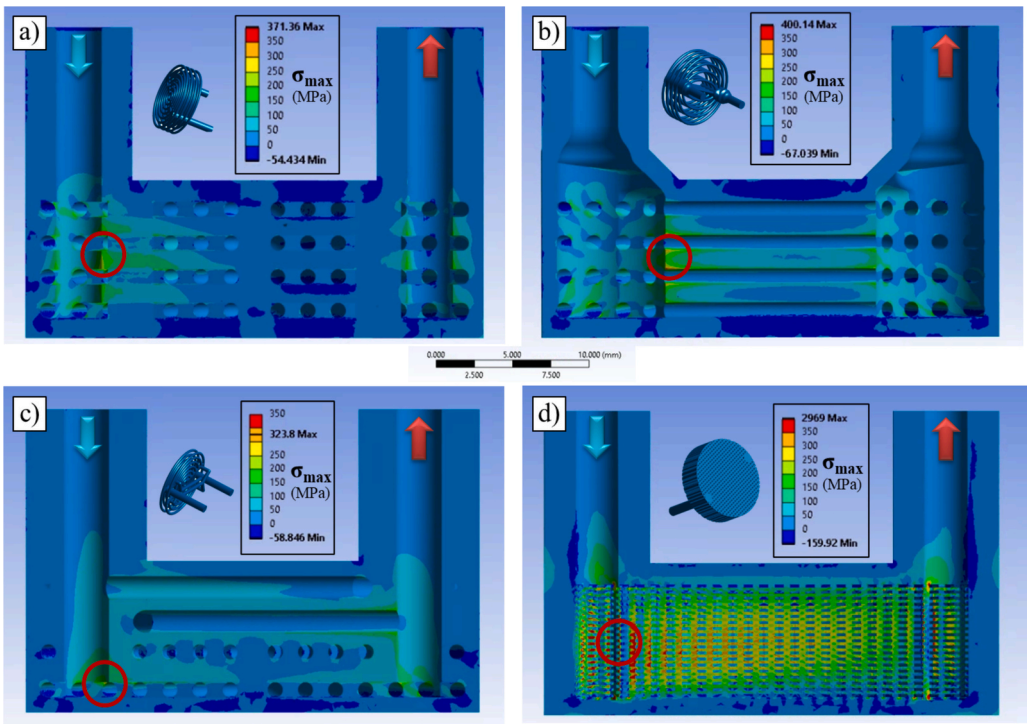

Fig. 7. Contour plots of the maximum principal tensile stress, σ_{max}, generated at the steady state in the ACTS system cooled by steam at 1 bar of pressure, shown for a) 4-layer circular, b) 4-layer oval, c) 2-layer circular and d) meshed designs, as indicated. Inlets and outlets are indicated by vertical blue and red arrows, respectively, and red circles indicate the areas where the maximum values in each contour plot are located. (For interpretation of the references to colour in this figure legend, the reader is referred to the web version of this article.)

Nevertheless, the differences between the front and back faces maximum temperatures depend strongly on the material selected for the fabrication of the ACTS system, as shown in Fig. 6 for the ACTS 2–layer circular design. Indeed, the difference becomes quite large (well over 1000 °C) when a material with low thermal conductivity like yttria-stabilized zirconia (YTZP) is used, and even the relatively milder 6–fold reduction in conductivity (from ~ 57 to ~ 9 W/m K at room temperature) resulting from substituting ZrB_2 for Inconel 718 alloy more than doubles the temperature differences between both faces. As clearly seen on this plot, such an increment is produced mostly by the increase in the maximum temperatures at the front face, with the back face temperatures remaining more or less unaltered, with the exception of YTZP at high flow rates, which exhibited a significant reduction in the maximum back face temperatures.

Two important ACTS manufacturing guidelines can be extracted from these results: high thermal conductivity is a critical parameter for reducing the maximum temperature at the heat-facing surfaces and a high temperature tolerance of the material would be critical to keep coolant mass flow requirements low for aerospace applications. Indeed, the 1573 K softening temperature of Inconel 718 (Greene and Finfrock, 2000) implies that around 0.34 g/s of dry steam would be necessary to avoid degradation of a thermal shield fabricated with this material under the heating conditions selected for this study. In contrast, the higher threshold for active oxidation of ZrB_2 materials, estimated to be around 1800 K in a recent study for additively manufactured parts (Charpentier et al., 2024), reduces the coolant flow required to prevent TPS degradation by more than 30%. Of course, passive insulation at the back face of the ACTS would be needed to shield the rest of the system from the still high temperatures in the back face of ACTS, but commercial lightweight and low-cost insulation materials capable to withstand such backface temperatures without any significant degradation are readily available. However, resistance to degradation at high temperature has to be combined with a high thermal conductivity, as is the case for ZrB_2 UHTCs. Indeed, while YTZP could potentially withstand

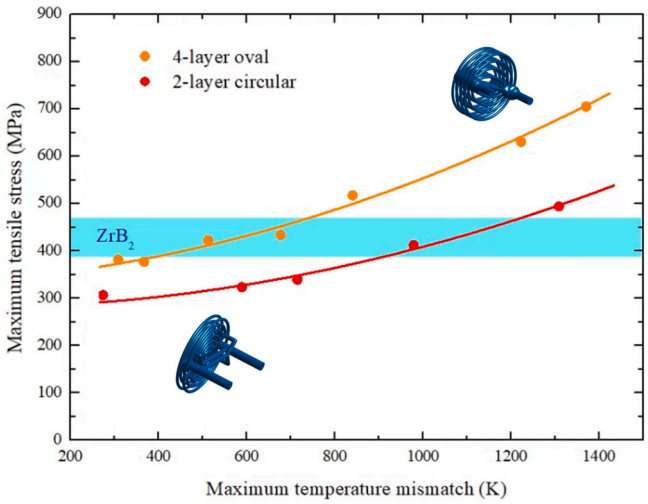

Fig. 8. Maximum tensile stress value generated at the steady state in the 4-layer oval and 2–layer circular ACTS designs cooled by steam as a function of the maximum temperature mismatch between the solid and the cooling fluid. Strength range for ZrB_2 from literature values (Neuman et al., 2013; Swab et al., 2023) is included as a horizontal shaded bar for comparison.

temperatures well in excess of 2400 K, such better performance is overshadowed by its lower thermal conductivity and, again, requires nearly twice the mass flow rate of ZrB_2 to withstand the heating conditions imposed in the present numerical analysis.

According to the previous analysis, ZrB_2 and other UHTCs appear as very good candidates for the fabrication of ACTS solutions, as proposed in this study, thanks to their outstanding combination of high thermal conductivity and high temperature resistance. This is especially true when their oxidation resistance is improved through the use of $MoSi_2$ or

SiC additives (Hwang et al., 2007; Sciti et al., 2005). Of course, one of the main drawbacks of UHTCs, which might be preventing a more widespread adoption for this type of TPS applications, is their intrinsic brittleness. Therefore, an evaluation and optimization of the mechanical stresses generated in the proposed ACTS systems is paramount, in order to avoid cracking under service-like conditions. For this purpose, a preliminary FEM mechanical analysis of the ZrB_2 ACTS systems was performed using the temperature distribution calculated in the CFD simulations as thermal loads for the system. Fig. 7 shows contours corresponding to the maximum principal stress—which would be responsible for any brittle cracking in the system—calculated for each of the evaluated designs, as indicated.

As shown in these contours, the maximum stresses in these systems are localized in the region where the inlet channel branches into the smaller horizontal channels around mid-thickness of the ACTS disk. This is precisely the region where the largest temperature gradients are found in the system, produced by the contact between the cool liquid and the hotter solid at the front face. This preliminary study also shows how sharp corners act as stress concentrators that need to be avoided in the design of the ACTS whenever possible. Indeed, the square-section channel features of the meshed design (Fig. 7d) are less desirable than the circular channels in the other 3 designs, exhibiting maximum stresses, located at the channel corners where those meet the inlet channel, almost an order of magnitude higher (~ 2.9 GPa) than the values calculated for the rest of the models. It is worth mentioning, though, that the selected element sizes—which were optimized in the 4-layer circular design but kept for all designs for the sake of comparability—might be too coarse to accurately capture the mechanical behaviour in a design with such small channel features. In any case, avoidance of sharp corners is always advisable when designing parts made from brittle materials like ZrB_2.

Of all analysed designs, the 2-layer circular design, exhibited the lowest level of thermal expansion related stresses, with the maximum displaced to the layer of channels closest to the front face. This is attributed to the absence, in this particular case, of small channels close to the location of the maximum temperature gradient in this design. The presence of much smaller channels in this same region in the meshed design might also contribute to the substantially larger stresses developed in such case (Fig. 7d). If that is the case, designing a more progressive branching of the channels, with larger manifolds and rounded edges close to the location of the maximum temperature gradients, will prove beneficial for reducing the developed stresses and minimizing the chance of failure of the ACTS system during service.

As shown in Fig. 8 for the 2-layer circular and 4-layer oval designs, the maximum stresses developed in the system exhibit a good correlation with the maximum temperature mismatch between the solid and the cooling fluid (steam)—calculated as the maximum temperature at the front face of the ACTS minus the fluid temperature at the inlet. Especially for the 4-layer oval designs, the calculated maximum stresses may exceed the strength of ZrB_2 UHTCs at low temperatures (under 1200 °C, the relevant range at the stress maximum location), which are in the 390–470 MPa range (Neuman et al., 2013; Swab et al., 2023). Therefore, avoiding cracking of the ACTS when produced from UHTCs could be an important challenge. This is especially true when the coolant mass flow needs to be kept to a minimum and, thus, the temperature mismatch increases.

Design optimization may play an important role in solving this problem, but material optimization would also be critical. Indeed, it is possible to enhance the mechanical strength of ZrB_2 with the addition of SiC, WC, ZrC and other phases as reinforcement, to values well in excess of 600 MPa (Zou et al., 2012; Zhang et al., 2011) that could withstand the developed stresses even at the highest temperature mismatch depicted in Fig. 8, at least for the 2-layer circular design. Indeed, such composites are often preferred for ultra-high temperature applications. The selection of pure ZrB_2, instead, for the numerical study was for reasons of availability of the complete set of temperature-dependent thermomechanical properties (thermal conductivity, heat capacity, thermal expansion coefficient, elastic modulus, etc.) required for the simulation of the UHTC material rather than an optimal performance. In any case, it is also worth noting that nominal strength values of the UHTC materials could be reduced due to flaws during the additive manufacturing process required to produce such microchannel-based structures; and that the presence of reinforced phases would also modify (positively or negatively) the actual stresses induced in the system as parameters such as thermal conductivity will also be affected by their presence.

Another sensible strategy to prevent fracture in the ACTS system would be to fabricate a functionally graded materials (FGM), with a brittle UHTC at the external heat-facing surface and a tougher material,

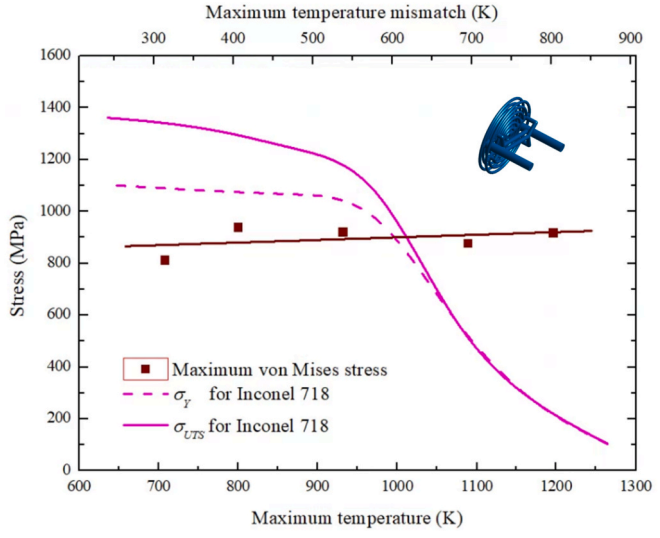

Fig. 9. Maximum von Mises stress value generated at the steady state in a purely elastic Inconel 718 ACTS system, with 2-layer circular design and cooled by steam, as a function of the maximum temperature (temperature mismatch is included at the top for comparison with Fig. 8). Inconel 718 yield stress and ultimate tensile strength values as a function of temperature are also included from literature (Davis, 2000).

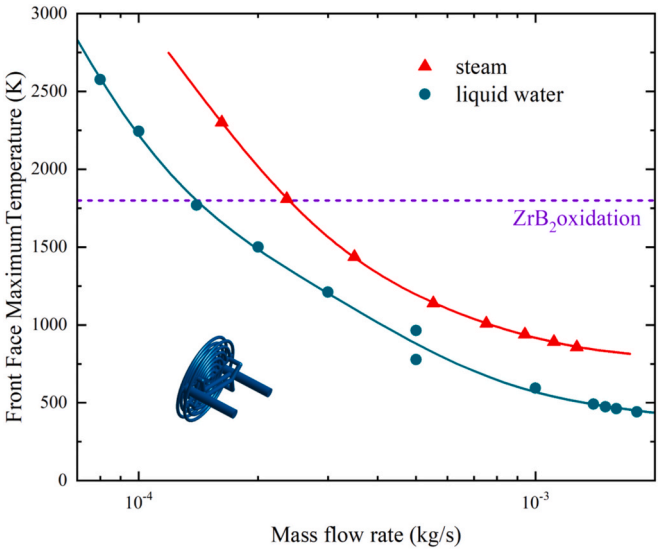

Fig. 10. Maximum temperature at the front face of a 2 layers circular design ZrB_2 ACTS as a function of the mass flow rate of dry steam or liquid water, as indicated. Oxidation temperature threshold for ZrB_2 is indicated as a horizontal dashed line.

like a high temperature alloy underneath it. Certainly, as shown in Fig. 7, the maximum stress occurs far from the external surface, in regions of the ACTS where temperatures are substantially lower than at the front face and therefore the material requirements in terms of heat resistance are less stringent. The consortium of the project AM–ACTS is already working on the development of strategies suitable for the fabrication of such FGM between ZrB_2 and Inconel 718 through additive manufacturing (Ratnala et al., 2023). Such a strategy may enable the fabrication of engineering parts capable of withstanding the stringent thermomechanical conditions that the proposed ACTS need to endure. Nonetheless, this strategy will have to be carefully optimized since the stresses developed when the ACTS structure is fabricated entirely with Inconel 718 are nearly triple compared to ZrB_2 counterparts, according to the simulations results obtained considering a purely elastic behaviour for the Ni-based alloy, which are summarized in Fig. 9. Such a notable stress increment, due to the substantially larger expansion coefficient of the metal, might jeopardize the structural integrity of the system despite the higher ductility and toughness of the metal, especially under the cyclic loading conditions required for a reusable ACTS. As shown in Fig. 9, the von Mises stresses developed in 2-layer circular ACTS structures made of Inconel 718 remain below the yield stress of the material at low temperature. However, such stresses tend to grow slowly with the temperature mismatch or maximum temperature in the system while the yield stress and ultimate tensile strength of Inconel 718 diminishes dramatically above 950 K, falling below the maximum developed stresses above 1000 K. This may impose a limit about how close to the areas of maximum temperature in the ACTS system the superalloy might be used in a multi-material structure. In case the superalloy was used to fabricate the whole ACTS system, it could also impose a more stringent limit to the maximum allowable temperatures and, thus, imply an increase in the coolant mass flow rate (cf. Fig. 6) required to preserve the mechanical integrity of the ACTS system in service conditions.

In any case, both the FEM and CFD analyses performed indicate that the 2-layer circular design provides improved cooling and mechanical performance for the ACTS system and suggest that ZrB_2 UHTCs are suitable candidate material for the applications. However, in order to evaluate the predicted overall performance of such a system, it is worth noting that steam at over 100 °C is not the optimal cooling agent. A more logical choice would be to use cool water since liquid water should be more readily available, and it will significantly outperform steam as a coolant thanks to its larger heat coefficient and latent heat of vaporization. Thus, previously presented results provide only a very conservative estimate of the level of cooling that can be achieved by using water as a coolant. Accordingly, multiphase simulations using the volume of fluid (VOF) model were conducted to evaluate the cooling effect produced by liquid water injected at the inlet at a temperature just above its melting point (273.15 K). Simulations were made exclusively for the 2-layer circular ACTS design, which exhibited the optimal cooling and mechanical performance according to Figs. 4b, 7 and 8. Although multiphase simulations are prone to convergence issues, this was avoided by selecting a relatively low (default) value of 0.1 s^{-1} for Lee model's mass transfer intensity factor (Miranda, 2021) and by patching an initial steam volume fraction in the fluid domain of 0 or 1, depending on which was closer to the final expected average value, as well as an initial temperature of 373 K close to the saturation temperature in the whole system. Fig. 10 summarise the findings of these simulations, showing a significant reduction, between 300 and 500 K, in the maximum front face temperature developed in the ACTS system at any given mass flow rate. Water vaporization entails a heat dissipation equivalent to an increase in the liquid water temperature $\Delta T_{vap} = h_{vap}/c_p \sim 500$ K, where h_{vap} is the latent heat of vaporization and c_p is the liquid water's specific heat coefficient. As observed in Fig. 10, ΔT_{vap} is of the order of the reduction in the maximum temperature achieved when water boils in the shield, indicating that this factor produces a significant effect. This additional temperature reduction allows to nearly halve (from 0.24 g/s to 0.14 g/s) the minimum mass flow rate of water required to keep the system below the active oxidation threshold for ZrB_2.

Considering this mass flow rate and the front face area (~700 mm^2) of the simulated heat shield element, the total water mass per minute necessary to cool the proposed ZrB_2 ACTS to tolerable limits at the assumed heat flow of 1 MW/m^2 would be in the order of 20 kg/m^2. For the same heating regime, an ablative phenolic carbon shield will lose a mass of approximately 2 kg/m^2 per minute (Kato et al., 2016). Of course, the adiabatic boundary conditions imposed here in the CFD simulations are more stringent than the actual situation—in which the ablative shields mass loss was evaluated—where some of the heat is transferred to the spacecraft frame and reradiated, so the actual coolant needs could be significantly reduced. In any case, it is expected that the use of the proposed actively cooled heat shields would still involve a certain weight penalty compared to state-of-the-art TPS solutions in aerospace applications, especially when the weight of the ACTS itself and the necessary backface insulation are taken into account. However, since the water used for this cooling process could have been previously employed for other purposes (life support, radiation shielding, etc.) within the ship, coolant mass might not have such a critical impact on the mission payload, at least for crewed missions.

Nevertheless, the proposed ACTS system will provide a TPS solution suitable for rapidly reusable spacecraft which cannot wait for the costly, labour-intensive and time-consuming process of ablative shield removal and re-application (Kennedy et al., 2024). Moreover, the self-heated steam resulting from ACTS cooling could be ejected at high speeds through appropriate nozzles at the front of the re-entering spacecraft for propulsive breaking, or at low speed through microvents or a porous material for evaporative and film cooling (Hermann et al., 2019; Shine and Nidhi, 2018). Self-adaptive transpiration cooling systems using the coolant phase change and expansion as a self-pumping mechanism could be designed (Dong et al., 2023), where high thermal conductivity rods/plates would transfer the incoming heat to a liquid water reservoir to form the required vapour outflow. This would significantly reduce the weight of the overall cooling and thermal protection system required to prevent deleterious degradation of the ACTS, since accelerated breaking would reduce the time the TPS has to withstand the extreme heating, and the protective cooling film would further reduce the maximum temperature in the ACTS.

To finalize the discussion, it is worth pointing out again that all absolute values calculated in this work must be used with care since the actual values in an application could change significantly due to differences in the boundary conditions or material properties hereby selected. This limitation, however, does not affect the validity of the design guidelines derived from the comparative study performed, which could be readily considered in the design of any actual high temperature thermal protection system.

4. Conclusions

A novel solution for the design of reusable thermal protection systems capable of sustaining extreme heating conditions of atmospheric re-entry shields for spacecrafts is proposed and analysed. The proposed solution consists of microchannel based thermal shields, fabricated using additive manufacturing from ultra-high temperature materials, that can be actively cooled. The level of cooling that can be achieved by circulating a suitable cooling fluid through a bioinspired internal microchannel network and the thermal stresses developed in the TPS material have been analysed with the aid of computational fluid dynamics and finite element modelling. Based on the analysis of these computational results, the following conclusions can be drawn:

Although microchannel design has a major effect on the pressure difference needed to achieve a given level of cooling in the ACTS, it has a minor effect on the mass flow rate of coolant needed, which is a more relevant parameter in aerospace applications.

High temperature tolerance and high thermal conductivity are the key material requirements for keeping the maximum temperatures at the heat-facing surface of the ACTS below acceptable levels. Thus, UHTC materials such as ZrB_2 appear to be optimal candidates for this application.

Cracking of the ZrB_2 UHTC materials may be an issue in ACTS applications and careful optimization of the design—aiming at avoiding stress concentrations at sharp corners or the presence of small channels around the regions of maximum temperature gradients in the system—as well as of the material itself, to maximize its strength, would be necessary to ensure survival of the system under the cyclic thermal loading conditions required for reusability.

Liquid water appears as a suitable coolant candidate for ACTS applications given its high thermal capacity and latent heat of vaporization. Moreover, its availability in crewed spacecrafts given its many other applications (life-support, radiation shielding, etc.) makes it an obvious choice for aerospace applications.

The water mass per unit area required for the ACTS to survive at a given heating level is about one order of magnitude higher than the mass loss produced by ablation on a state-of-the-art phenolic carbon shield under similar heating conditions. However, the high cost and single-use of the latter may make the water-cooled ACTS a more desirable solution for reusable spacecrafts, especially considering the multiple additional uses such water may have.

CRediT authorship contribution statement

Pedro Miranda: Writing – review & editing, Writing – original draft, Software, Project administration, Methodology, Investigation, Funding acquisition, Conceptualization. **Rafael Agujetas:** Validation, Software, Methodology, Formal analysis. **José M. Montanero:** Writing – review & editing, Validation, Methodology, Formal analysis. **Florencia M. Nogales:** Visualization, Software, Investigation. **Abdulnaser Sayma:** Writing – review & editing, Validation, Supervision, Software, Resources, Formal analysis.

Declaration of competing interest

The authors declare the following financial interests/personal relationships which may be considered as potential competing interests: [Pedro Miranda reports financial support was provided by State Agency of Research. If there are other authors, they declare that they have no known competing financial interests or personal relationships that could have appeared to influence the work reported in this paper.].

Acknowledgments

This study was carried out in the framework of the M-ERA.Net3 project AM-ACTS, grant PCI2022-132933, funded by MCIN/AEI/10.13039/501100011033 and the European Union NextGenerationEU/PRTR. The authors would like to acknowledge Prof. Jafar Al-Zaili and the rest of colleagues at City University of London for helpfully hosting the first author at their facilities during part of this research execution.

Data availability

Data will be made available on request.

References

Schütze, M., 2000. Fundamentals of high temperature corrosion. Materials Science and Technology: A Comprehensive Treatment 67–130. 10.1002/9783527619306.ch2.

Thakare, J.G., Pandey, C., Mahapatra, M.M., Mulik, R.S., 2020. Thermal barrier coatings—a state of the art review. Met. Mater. Int. https://doi.org/10.1007/s12540-020-00705-w.

Golla, B.R., Mukhopadhyay, A., Basu, B., Thimmappa, S.K., 2020. Review on ultra-high temperature boride ceramics. Prog. Mater Sci. 111, 100651. https://doi.org/10.1016/j.pmatsci.2020.100651.

Justin, J.F., Jankowiak, A., 2011. Ultra high temperature ceramics: densification, properties and thermal stability. AerospaceLab 3, AL3-08. https://hal.science/hal-01183657.

Fahrenholtz, W.G., Hilmas, G.E., 2017. Ultra-high temperature ceramics: Materials for extreme environments. Scr. Mater. 129, 94–99. https://doi.org/10.1016/j.scriptamat.2016.10.018.

K.N. S, S. Rao Bakshi, Reactive spark plasma sintering and mechanical properties of zirconium diboride-titanium diboride ultrahigh temperature ceramic solid solutions, Technologies 4 (2016) 30. https://doi.org/10.3390/technologies4030030.

Zamora, V., Ortiz, A.L., Guiberteau, F., Nygren, M., 2012. Crystal-size dependence of the spark-plasma-sintering kinetics of ZrB2 ultra-high-temperature ceramics. J. Eur. Ceram. Soc. 32, 271–276. https://doi.org/10.1016/j.jeurceramsoc.2011.08.027.

Zamora, V., Ortiz, A.L., Guiberteau, F., Nygren, M., 2012. Spark-plasma sintering of ZrB2 ultra-high-temperature ceramics at lower temperature via nanoscale crystal refinement. J. Eur. Ceram. Soc. 32, 2529–2536. https://doi.org/10.1016/j.jeurceramsoc.2012.02.023.

Sciti, D., Pienti, L., Natali Murri, A., Landi, E., Medri, V., Zoli, L., 2014. From random chopped to oriented continuous SiC fibers-ZrB2 composites. Mater. Des. 63, 464–470. https://doi.org/10.1016/j.matdes.2014.06.037.

Dehdashti, M.K., Fahrenholtz, W.G., Hilmas, G.E., 2014. Effects of temperature and the incorporation of W on the oxidation of ZrB2 ceramics. Corros. Sci. 80, 221–228. https://doi.org/10.1016/j.corsci.2013.11.030.

Hu, P., Zhang, X.-H., Han, J.-C., Luo, X.-G., Du, S.-Y., 2010. Effect of various additives on the oxidation behavior of ZrB2-based ultra-high-temperature ceramics at 1800 °C. J. Am. Ceram. Soc. 93, 345–349. https://doi.org/10.1111/j.1551-2916.2009.03420.x.

Huo, C., Guo, L., Zhou, L., Liu, B., Wang, C., Zhang, Y., Wang, H., 2018. Effect of Al2O3 addition on the ablation behavior of SiC-ZrC coated C/C composites. J. Alloy. Compd. 752, 489–504. https://doi.org/10.1016/j.jallcom.2018.04.091.

T.A. Hermann, I. Naved, M. McGilvray, Performance of transpiration cooled heat shields for hypersonic vehicles, in: AIAA Scitech 2019 Forum, American Institute of Aeronautics and Astronautics, 2019. https://doi.org/doi:10.2514/6.2019-1778.

Shine, S.R., Nidhi, S.S., 2018. Review on film cooling of liquid rocket engines. Prop Power Res 7, 1–18. https://doi.org/10.1016/j.jppr.2018.01.004.

Kennedy, A., McNulty, Z., Nutt, S., 2024. Producing ablative thermal protection systems by additive manufacturing. Advanced Manufacturing: Polymer and Composites Science 10. https://doi.org/10.1080/20550340.2024.2366622.

Badea, T.A., Maier, L.R., Crisan, A.A., 2025. Assessment of additively manufactured thermoplastic composites for ablative thermal protection systems (TPSs). Polymers 17, 2338. https://doi.org/10.3390/POLYM17172338.

Olson, N., Boghozian, T., Sidor, A., Larsen, G., Bouslog, S., Venkatapathy, E., 2023. Development of additive manufacturing technologies for 3D printing of spacecraft heat shields, CME NASA. Symposium. https://ntrs.nasa.gov/citations/20230012013.

DJ Blette, AT Sidor, JE Theisinger, AD Omidy, Overview of additively manufactured TPS proposed flight test and earth re-entry capsule design, 2024 IEEE Aerospace Conference, Big Sky, MT, USA, 2024, pp. 1-11 doi: 10.1109/AERO58975.2024.10521445.

Mei, H., Li, H., Jin, Z., Li, L., Yang, D., Liang, C., Cheng, L., Zhang, L., 2023. 3D-printed SiC lattices integrated with lightweight quartz fiber/silica aerogel sandwich structure for thermal protection system. Chem. Eng. J. 454, 140408. https://doi.org/10.1016/J.CEJ.2022.140408.

K.M. Raisch, Additive manufacturing of ceramic composites for thermal protection systems, (2020). https://hdl.handle.net/10945/65427.

Ferrari, L., Barbato, M., Esser, B., Petkov, I., Kuhn, M., Gianella, S., Barcena, J., Jimenez, C., Francesconi, D., Liedtke, V., Ortona, A., 2016. Sandwich structured ceramic matrix composites with periodic cellular ceramic cores: an active cooled thermal protection for space vehicles. Compos. Struct. 154, 61–68. https://doi.org/10.1016/J.COMPSTRUCT.2016.07.043.

Hatton, B.D., Wheeldon, I., Hancock, M.J., Kolle, M., Aizenberg, J., Ingber, D.E., 2013. An artificial vasculature for adaptive thermal control of windows. Sol Energy Mater Sol Cell 117, 429–436. https://doi.org/10.1016/j.solmat.2013.06.027.

Tao, P., Shang, W., Song, C., Shen, Q., Zhang, F., Luo, Z., Yi, N., Zhang, D., Deng, T., 2015. Bioinspired engineering of thermal materials. Adv. Mater. 27, 428–463. 10.1002/adma.201401449.

Van Erp, R., Soleimanzadeh, R., Nela, L., Kampitsis, G., Matioli, E., 2020. Co-designing electronics with microfluidics for more sustainable cooling. Nature 585. https://doi.org/10.1038/s41586-020-2666-1.

F.M. Nogales, A.L. Ortiz, P. Miranda, Direct ink writing and pressureless spark plasma sintering of ultra-high temperature ceramics for the production of complex parts with internal microchannels, J Eur Ceram Soc Under review.

Sández-Gómez, Á., Ortiz, A.L., Miranda, P., 2025. Production of complex microchanneled parts of ZrB2-MoSi2 ultra-high temperature ceramics by freeze casting and pressureless spark plasma sintering. J. Eur. Ceram. Soc. 45. https://doi.org/10.1016/j.jeurceramsoc.2024.116966.

Scheithauer, U., Slawik, T., Schwarzer, E., Richter, H.J., Moritz, T., Michaelis, A., 2015. Additive manufacturing of metal-ceramic-composites by thermoplastic 3D-printing (3DTP). J Ceram Sci Technol 6, 125–132. https://doi.org/10.4416/JCST2014-00045.

Raynaud, J., Pateloup, V., Bernard, M., Gourdonnaud, D., Passerieux, D., Cros, D., Madrangeas, V., Michaud, P., Chartier, T., 2021. Hybridization of additive manufacturing processes to build ceramic/metal parts: example of HTCC. J. Eur. Ceram. Soc. 41, 2023–2033. https://doi.org/10.1016/j.jeurceramsoc.2020.10.032.

P. Miranda, AM-ACTS project website, https://am-acts.eu/ (2021).
Ernst, U., 1986. Schlünder. Hemisphere Publishing Corporation, Heat exchanger design handbook.
Grohsmeyer, R.J., Silvestroni, L., Hilmas, G.E., Monteverde, F., Fahrenholtz, W.G., D'Angió, A., Sciti, D., 2019. ZrB2 -MoSi2 ceramics: a comprehensive overview of microstructure and properties relationships. Part II: Mechanical Properties, J Eur Ceram Soc 39, 1948–1954. https://doi.org/10.1016/j.jeurceramsoc.2019.01.021.
Zimmermann, J.W., Hilmas, G.E., Fahrenholtz, W.G., Dinwiddie, R.B., Porter, W.D., Wang, H., 2008. Thermophysical properties of ZrB2 and ZrB2–SiC ceramics. J. Am. Ceram. Soc. 91, 1405–1411. https://doi.org/10.1111/j.1551-2916.2008.02268.x.
Lugovy, M., Slyunyayev, V., Orlovskaya, N., Mitrentsis, E., Aneziris, C.G., Graule, T., Kuebler, J., 2016. Temperature dependence of elastic properties of ZrB2-SiC composites. Ceram. Int. 42, 2439–2445. https://doi.org/10.1016/j.ceramint.2015.10.044.
Nakamori, F., Ohishi, Y., Muta, H., Kurosaki, K., Fukumoto, K.I., Yamanaka, S., 2015. Mechanical and thermal properties of bulk ZrB2. J. Nucl. Mater. 467, 612–617. https://doi.org/10.1016/j.jnucmat.2015.10.024.
K.C. Mills, Ni-IN718, in: Recommended values of thermophysical properties for selected commercial alloys, 2002: pp. 181–190.
Davis, J.R., 2000. ASM Specialty handbook: nickel, cobalt, and their alloys, ASM. International.
Radovic, M., Lara-Curzio, E., Trejo, R.M., Wang, H., Porter, W.D., 2008. Thermophysical Properties of YSZ and Ni-YSZ as a Function of Temperature and Porosity 79–85. https://doi.org/10.1002/9780470291337.ch8.
Limarga, A.M., Clarke, D.R., 2011. The grain size and temperature dependence of the thermal conductivity of polycrystalline, tetragonal yttria-stabilized zirconia. Appl. Phys. Lett. 98. https://doi.org/10.1063/1.3593383.
Hirt, C.W., Nichols, B.D., 1981. Volume of fluid (VOF) method for the dynamics of free boundaries. J. Comput. Phys. 39, 201–225. https://doi.org/10.1016/0021-9991(81)90145-5.
W.H. Lee, A pressure iteration scheme for two-phase flow modeling, in: Computational methods for two-phase flow and particle transport, World Scientific, 2013: pp. 61–82. https://doi.org/10.1142/9789814460286_0004.
Chen, G., Nie, T., Yan, X., 2020. An explicit expression of the empirical factor in a widely used phase change model. Int. J. Heat Mass Transf. 150, 119279. https://doi.org/10.1016/j.ijheatmasstransfer.2019.119279.
G.A. Greene, C.C. Finfrock, Oxidation of Inconel 718 in air at temperatures from 973K to 1620K., Upton, NY, 2000. https://doi.org/10.2172/777719.
Charpentier, L., Miranda, P., Tallaron, H., Nogales, F.M., Sández-Gómez, Á., Bêche, E., Balat-Pichelin, M., 2024. The oxidation of ZrB2/MoSi2 ceramics in dissociated air: the influence of the elaboration technique. Materials 17, 3818. https://doi.org/10.3390/ma17153818.
Hwang, S.S., Vasiliev, A.L., Padture, N.P., 2007. Improved processing and oxidation-resistance of ZrB2 ultra-high temperature ceramics containing SiC nanodispersoids. Mater. Sci. Eng. A 464, 216–224. https://doi.org/10.1016/j.msea.2007.03.002.
Sciti, D., Brach, M., Bellosi, A., 2005. Oxidation behavior of a pressureless sintered ZrB2–MoSi2 ceramic composite. J. Mater. Res. 20, 922–930. https://doi.org/10.1557/JMR.2005.0111.
Neuman, E.W., Hilmas, G.E., Fahrenholtz, W.G., 2013. Strength of zirconium diboride to 2300 °C. J. Am. Ceram. Soc. 96, 47–50. https://doi.org/10.1111/jace.12114.
Swab, J.J., Jarman, J., Fahrenholtz, W., Watts, J., 2023. Mechanical properties of ZrB2 ceramics determined by two laboratories. Int. J. Appl. Ceram. Technol. 20, 3097–3103. https://doi.org/10.1111/ijac.14429.
Zou, J., Zhang, G., Hu, C., Nishimura, T., Sakka, Y., Vleugels, J., Van der Biest, O., 2012. ZrB2–SiC–WC ceramics at 1600 °C. J. Am. Ceram. Soc. 95, 874–878. https://doi.org/10.1111/j.1551-2916.2011.05062.x.
Zhang, S.C., Hilmas, G.E., Fahrenholtz, W.G., 2011. Mechanical properties of sintered ZrB2–SiC ceramics. J. Eur. Ceram. Soc. 31, 893–901. https://doi.org/10.1016/j.jeurceramsoc.2010.11.013.
Ratnala, D.C., Andersson, J., Joshi, S., 2023. Development of functionally graded metal-ceramic systems by directed energy deposition: a review. Mater. Sci. Forum 1107, 105–110. https://doi.org/10.4028/p-4ekAtd.
Kato, S., Matsuda, S., Okuyama, K., Gibo, K., Oya, H., Watanabe, A., Shimada, N., Sakai, S., 2016. Study of the effects of heat load, ablator density and backup structure upon the thermal protection performance of heat shield systems consisting of phenolic carbon ablators. Trans Jpn Soc Aeronaut Space Sci, Aerospace Tech Jpn 14, 95–104. https://doi.org/10.2322/tastj.14.Pe_95.
Kennedy, A., McNulty, Z., Nutt, S., 2024. Producing ablative thermal protection systems by additive manufacturing, Adv Manuf. Polym Compos Sci 10. https://doi.org/10.1080/20550340.2024.2366622.
Dong, W., Deng, P., Lin, S., Chen, T., 2023. Numerical study of a new scheme of self-adaptive transpiration cooling. Appl. Therm. Eng. 230, 120779. https://doi.org/10.1016/j.applthermaleng.2023.120779.